European Congress on Computational Methods in Applied Sciences and Engineering
ECCOMAS 2004
P. Neittaanmäki, T. Rossi, K. Majava, and O. Pironneau (eds.)
W. Rodi and P. Le Quéré (assoc. eds.)
Jyväskylä, 24—28 July 2004

COMPUTATIONAL HAEMODYNAMICS AND THE EFFECTS OF BLOOD RHEOLOGICAL MODELS ON THE FLOW THROUGH AN ARTERIAL STENOSIS

Panagiotis Neofytou* **and Sokrates Tsangaris†**

School of Mechanical Engineering, Fluids Section, National Technical University of Athens, 15710 Zografou, Athens, Greece

* e-mail: panos_n@hotmail.com,
† e-mail: sgt@fluid.mech.ntua.gr

Key words: Haemodynamics, CFD, Non-Newtonian flows, Blood rheological models, Stenosis.

Abstract. *The effects of different blood rheological models are investigated numerically utilising a three-dimensional model of a stenosis. The employed CFD code incorporates the SIMPLE scheme in conjunction with the finite volume method with collocated arrangement of variables. The approximation of the convection terms is carried out using the QUICK differencing scheme whereas the code enables also multi-block computations, which are useful in order to cope with the two-block grid structure of the current computational domain. Three non-Newtonian models are employed, namely the Casson, Power-Law and Quemada models, which have been introduced in the past for modelling the rheological behaviour of blood and cover both the viscous as well as the two-phase character of blood. In view of the haemodynamical mechanisms related to atherosclerosis formation and the role of the wall shear stress in initiating and further developing of the disease, the present study focuses on the three-dimensional flow field and in particular on the distribution as well as on both low and high values of the wall shear stress in the vicinity of the stenosis. Finally, a comparison is made between the effects of each rheological model on the aforementioned parameters. Results show marked differences between simulating blood as Newtonian and as non-Newtonian fluid and furthermore that the Power-Law model exhibits in general different trends compared to the Quemada and Casson models as regards to the flow field and wall shear stress when the Reynolds number or degree of stenosis alter, whereas the behaviour of the Quemada and Casson models is similar.*

1 INTRODUCTION

The presence of a partial occlusion in the human circulatory system may substantially alter the flow field and subsequently the flow rate of blood leading to severe incidences such as cardiac arrest and stroke. The role of fluid dynamics in the arterial network and furthermore in the development of atherosclerosis formation involving three-dimensional geometry setups has been under investigation for many years.

Ang and Mazumdar [1] used Computational Fluid Dynamics (CFD) in order to model the flow in a vessel with an asymmetric stenosis and study the shear-stress distribution in the vicinity of the occlusion. Their results show that the peak shear stress varies only slightly with the Reynolds number. Numerical simulation of the flow in an asymmetric geometry was also performed by Dvinsky and Ojha [2] in order to validate their code and complement previous experimental results. Bethier *et al.* [3] numerically solved the flow in a realistic 3D reconstruction of the human right coronary artery focusing on the effects of the reconstruction methods. They showed that the local flow patterns are severely affected by the geometrical modifications. Axisymmetric and asymmetric 3D stenotic models were used by Long *et al.* [4] to study the flow separation zone and the wall shear-stress distribution in the poststenotic region involving three degrees of area reduction and using a realistic pressure waveform as inlet condition. Their results show a complexity of the flow patterns especially in the flow deceleration phase. The phenomenon of wall deformability was taken into account in the study by Tang *et al.* [5] where a 3D computational model with fluid wall interaction was introduced to investigate the flow in stenotic elastic tubes and to quantify wall collapse and related critical flow attributes and wall mechanical conditions.

In addition to numerical modelling, experimental studies regarding stenotic vessels were also performed by Deplano and Siouffi [6] using a water and glycerol mixture to simulate blood viscosity. Their experiments conclude that high shear-stress values at the throat of the constriction can imply more damage as plaque disruptions. Flow visualisation experiments in an axisymmetric stenotic vessel were also carried out by Bluestein *et al.* [7] showing that periodic vortex-shedding in the poststenotic region begins at approximately Re=375 and that the unsteady flow development in the recirculation region may be the mechanism for significant changes in the distribution of mural platelet deposition.

The aim of the present study is to investigate the effects of modelling the blood as non-Newtonian fluid in 3D flows as done in the past for 2D flows [8, 9, 10] employing three well documented blood rheological models namely the Casson [11], Power-Law [12] and Quemada [13] models. The investigation is carried out by numerically modelling the flow in a 3D axisymmetric model of a stenosis at different Reynolds numbers and degrees of stenosis.

2 MODEL

2.1 Governing equations

The flow is considered to be laminar and incompressible and therefore the Navier-Stokes equations for three-dimensional incompressible flow are used in their integral form in order to accommodate the subsequent finite-volume discretisation. These are the continuity

$$\int_S \boldsymbol{V}\cdot\boldsymbol{dS}=0 \tag{1}$$

where $\boldsymbol{V}=(u,v,w)$, u, v and w are the velocity components in the x, y and z directions respectively and momentum equations

$$\frac{\partial}{\partial t}\int_\Omega \rho u d\Omega+\int_S \rho u\boldsymbol{V}\cdot\boldsymbol{dS}=-\int_S p\boldsymbol{i}_x\cdot\boldsymbol{dS}+\int_S\left(\tau_{xx}\boldsymbol{i}_x+\tau_{xy}\boldsymbol{i}_y+\tau_{xz}\boldsymbol{i}_z\right)\cdot\boldsymbol{dS} \tag{2a}$$

$$\frac{\partial}{\partial t}\int_\Omega \rho v d\Omega+\int_S \rho v\boldsymbol{V}\cdot\boldsymbol{dS}=-\int_S p\boldsymbol{i}_y\cdot\boldsymbol{dS}+\int_S\left(\tau_{yx}\boldsymbol{i}_x+\tau_{yy}\boldsymbol{i}_y+\tau_{yz}\boldsymbol{i}_z\right)\cdot\boldsymbol{dS} \tag{2b}$$

$$\frac{\partial}{\partial t}\int_\Omega \rho w d\Omega+\int_S \rho w\boldsymbol{V}\cdot\boldsymbol{dS}=-\int_S p\boldsymbol{i}_z\cdot\boldsymbol{dS}+\int_S\left(\tau_{zx}\boldsymbol{i}_x+\tau_{zy}\boldsymbol{i}_y+\tau_{zz}\boldsymbol{i}_z\right)\cdot\boldsymbol{dS} \tag{2c}$$

for the x, y and z directions respectively. Ω represents volume; $\boldsymbol{dS}$ equals to $\boldsymbol{n}\cdot dS$ where $\boldsymbol{n}$ is the unit vector normal to the surface dS; $\boldsymbol{i}_x$, $\boldsymbol{i}_y$, $\boldsymbol{i}_z$ are the unit vectors in the x, y and z directions, respectively; p is the pressure and ρ is the density. Following the analysis in [10] the shear-stress tensor in the diffusion terms is expressed in the case of non-Newtonian fluids as

$$\bar{\boldsymbol{\tau}}=\mu(|\bar{\boldsymbol{\gamma}}|)\bar{\boldsymbol{\gamma}} \tag{3}$$

where $\bar{\boldsymbol{\gamma}}$ is the shear-rate tensor and μ is the viscosity expressed as a function of the second invariant of $\bar{\boldsymbol{\gamma}}$.

The constitutive equations for modelling the shear thinning attributes of blood are expressed in 3D form as follows:

(*i*) Casson model: Due to its discontinuous character the application of the Casson model [11] in numerical schemes is difficult. Papanastasiou [14] proposed an alternative expression for the whole range of shear-stress values that therefore overcomes this obstacle. Expressed according to (3) this equation becomes:

$$\bar{\boldsymbol{\tau}}=\left[\sqrt{\mu_\infty}+\sqrt{\frac{\tau_y}{|\bar{\boldsymbol{\gamma}}|}}\left(1-e^{-\sqrt{m|\bar{\boldsymbol{\gamma}}|}}\right)\right]^2\bar{\boldsymbol{\gamma}} \tag{4}$$

where m>100 for satisfactory approximation. The dimensionless expression of (4) is

$$\bar{\boldsymbol{\tau}}^*=\frac{1}{\mathrm{Re}_{\mathrm{CA}}}\left[1+\sqrt{\frac{\mathrm{Bi}}{|\bar{\boldsymbol{\gamma}}|^*}}\left(1-e^{-\sqrt{m|\bar{\boldsymbol{\gamma}}|^*}}\right)\right]^2\bar{\boldsymbol{\gamma}}^* \tag{5}$$

where the asterisk superscript denotes dimensionless quantities and

$$\mathrm{Re}_{\mathrm{CA}}=\frac{\rho U_\infty D}{\mu_\infty},\quad \mathrm{Bi}=\frac{\tau_y D}{\mu_\infty U_\infty} \tag{6}$$

are the Reynolds and Bingham numbers respectively and are the characteristic parameters for a Casson-model flow.

(*ii*) Power-Law model: Based on this model Walburn and Schneck [12] developed a constitutive equation for blood where in exponent n and parameter k of the model the Total Plasma Minus Albumin (TPMA) and the Haematocrit are taken into account. According to (3) the 3D dimensionless expression is

$$\bar{\boldsymbol{\tau}}^{*} = \frac{1}{\mathrm{Re}_{\mathrm{PL}}} \left|\bar{\boldsymbol{\gamma}}\right|^{*\,n-1} \bar{\boldsymbol{\gamma}}^{*} \tag{7}$$

where

$$\mathrm{Re}_{\mathrm{PL}} = \frac{\rho D^{n}}{k U_{\infty}^{n-2}} \tag{8}$$

is the Reynolds number and characteristic parameter for a Power-Law-model flow.

(*iii*) Quemada model: This model is developed by Quemada [13] for concentrated disperse systems. Based on (3) the 3D expression of the model becomes:

$$\bar{\boldsymbol{\tau}} = \mu_{F} \left(1 - \frac{1}{2} \frac{k_{o} + k_{\infty} \sqrt{\left|\bar{\boldsymbol{\gamma}}\right| / \gamma_{c}}}{1 + \sqrt{\left|\bar{\boldsymbol{\gamma}}\right| / \gamma_{c}}} \varphi \right)^{-2} \bar{\boldsymbol{\gamma}} \tag{9}$$

where μ_{F} the viscosity of plasma (suspending medium), φ is haematocrit and γ_{c}, k_{∞} , k_{o} are parameters determining the rheological behaviour of the model. The dimensionless expression of (9) is:

$$\bar{\boldsymbol{\tau}}^{*} = \frac{1}{\mathrm{Re}_{\mathrm{QU}}} \left(1 - \frac{1}{2} \frac{k_{o} + k_{\infty} \sqrt{\left|\bar{\boldsymbol{\gamma}}\right|^{*} / \gamma_{c}^{*}}}{1 + \sqrt{\left|\bar{\boldsymbol{\gamma}}\right|^{*} / \gamma_{c}^{*}}} \varphi \right)^{-2} \bar{\boldsymbol{\gamma}}^{*} \tag{10}$$

where

$$\mathrm{Re}_{\mathrm{QU}} = \frac{\rho U_{\infty} D}{\mu_{F}}, \quad \gamma_{c}^{*} = \frac{\gamma_{c}}{U_{\infty} / D} \tag{11}$$

are the characteristic parameters for a Quemada-model flow.

2.2 Geometry

The geometry consists of a tube of diameter D and can be divided in three segments namely the inlet segment with length $4D$, the axisymmetrically constricted segment with length $2D$ and the outlet segment with length $20D$. The radius R_0 of the inlet and outlet segments is undeformed and equal to $D/2$, whereas the radius of the constricted segment is given by

$$R = R_0\left(1-\mathrm{St}\left(\frac{1-\cos(\pi x/D)}{2}\right)^2\right),\ 0\le x\le 2D \tag{12}$$

where St is the degree of the stenosis defined by

$$\mathrm{St} = \frac{R_0 - R_{\min}}{R_0}\cdot 100\% \tag{13}$$

and $R_{\min}$ is the radius of the tube at the throat of the constriction. For the current study, three different degrees of stenosis were used namely 20%, 50% and 80%, the shape of which is shown in Figure 1.

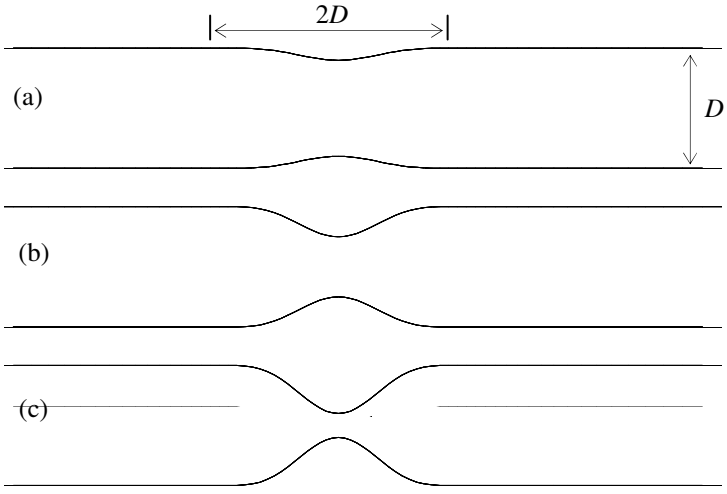

Figure 1: Different degrees of stenosis: (a) 20%; (b) 50%; (c) 80%

2.3 Conditions and parameters

Apart from the different degrees of stenosis the effects of the blood rheological models under consideration are studied for different Reynolds numbers. These are Re=100, 200 and 300. Due the fact that the Navier-Stokes equations are incorporated into the numerical scheme in their dimensionless form, the characteristic parameters in equations (6), (8) and (11) are to be calculated accordingly. For the Casson model and according to Charm *et al.* [15] for blood, τ_y=10.82mPa, μ_∞=3.1·10^{-3}Pa·s and ρ=1056kg/m^3. In addition, D=8mm in compliance with blood flow in carotid arteries [5]. Therefore, from $\mathrm{Re_{CA}}$ having the same definition as Re for Newtonian flows, the calculation of U_∞ from each of the aforementioned values of Re is possible and thus Bi can be calculated. For the Power-Law model the parameters in (8) according to Walburn and Schneck [12] are in the case of blood k=14.67·10^{-3}Pa·s^n and n=0.7755. Therefore according to calculation of U_∞, for each value of Re the corresponding value of $\mathrm{Re_{PL}}$ can be calculated. The parameters of Quemada model for blood [13] are γ_c=1.88s^{-1}, k_∞=2.07 and k_o=4.33. Therefore, in the same way as for the other models, the

values of Re_{QU} and γ_c^* can be calculated. Since D, ρ and μ_∞ are constant, the different Re values essentially correspond to different inlet flow rates, the mean value of which is U_∞.

The boundary conditions are constant velocity profile and pressure at the inlet and no-slip condition at the walls. At the outlet boundary the pressure and velocity are derived by extrapolation from the inner nodes. The velocity profile at the inlet is regarded to be that of the fully developed flow in a straight tube and can be derived analytically for Newtonian and Power-Law flows. Its dimensionless form is

$$u^* = 2\left[1-\left(\frac{r^*}{R_0^*}\right)^2\right],\ 0\le r^*\le R_0^* \tag{14}$$

for the Newtonian case and

$$u^* = \frac{1}{8}\frac{6n+2}{n+1}\left(\frac{1}{R_0^*}\right)^2\left[1-\left(\frac{r^*}{R_0^*}\right)^{\frac{n+1}{n}}\right],\ 0\le r^*\le R_0^* \tag{15}$$

for the Power-Law case. Due to the complex kind of the equations for the Quemada and Casson models, the fully developed flow used as inlet conditions for each of these cases is calculated numerically similarly as in [16].

3 NUMERICAL METHOD

3.1 Computational scheme

The code used for the calculations incorporates the finite volume method with collocated arrangement of variables on curvilinear grids and has been used in the past for 2D simulations [10, 16]. For coupling the momentum and continuity equations the pressure-correction method in conjunction with the SIMPLE scheme is applied. The newest feature is the incorporation of the QUICK [17] differencing scheme for the approximation of the convection terms in order to avoid the diffusive effects of the low order schemes. Furthermore, the code enables also multi-block computations, which are useful in order to cope with the two-block grid structure of the current computational domain (Fig. 2).

3.2 Grid

The grid used in the computations consists of hexahedral elements and is based on multiblock structure. The inner block is of a rectangular cross section and is encircled by the outer block as shown in Figure 2. Furthermore, the grid is locally refined near at constricted segment so that the anomalies in the flow field and the wall shear-stress (WSS) distribution caused by the constriction are captured in more detail.

A gird refinement study is also contacted and three grid resolutions were tested namely grid *a* with 39345 control volumes (CVs), grid *b* with 77108 CVs and grid *c* with 104160 CVs. The test is carried out for Newtonian flow and for a 50% degree of stenosis by

comparing the dimensionless WSS. It can be seen that the results for grids *b* and *c* are very close and therefore grid *b* is used for all further computations of this study.

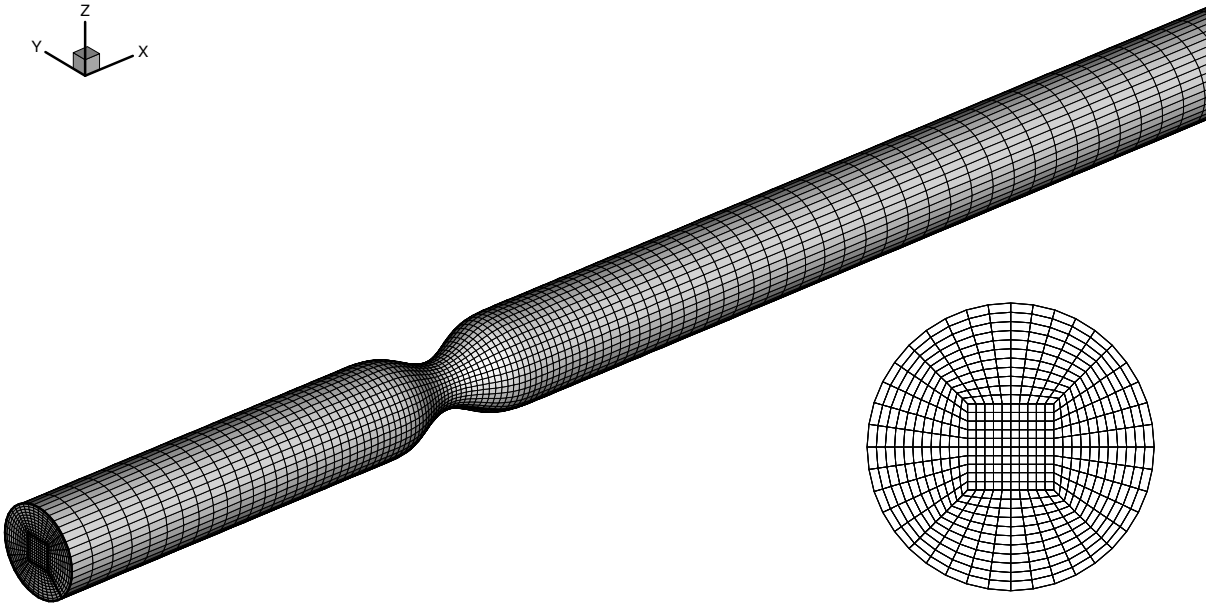

Figure 2: 3D grid with cross-section.

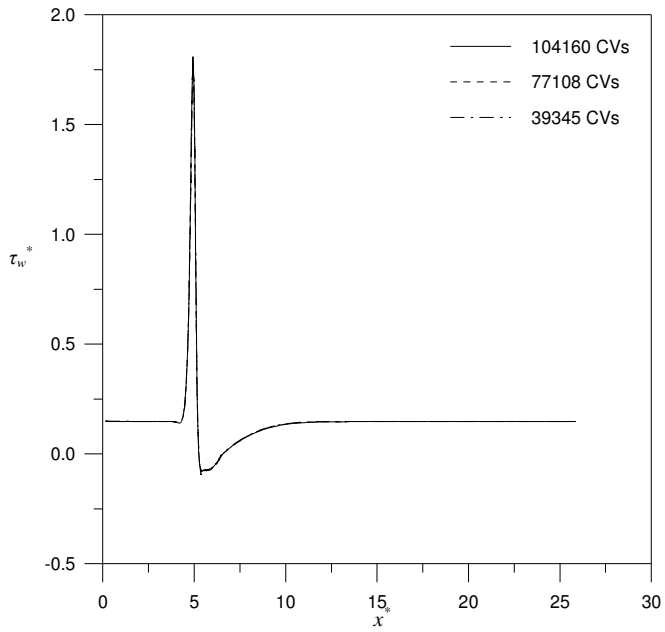

Figure 3: Grid refinement study by comparison of the dimensionless wall shear stress for three grid resolutions.

4 RESULTS AND DISCUSSION

Computations are contacted for three different Re numbers and three different degrees of stenosis so that the effects of the blood rheological model on important flow aspects such as the flow field and WSS distribution are determined. The effect of different Re numbers was studied for a 50% degree of stenosis whereas the effect of the stenosis degree was studied for Re=100. From a value of Re the velocity U_∞ is calculated from Re_{CA} and then used to calculate the rest of the parameters in (6), (8) and (11). Therefore the intercomparison between the models for a specific value of Re implies intercomparison for the same inlet flow rate.

4.1 Effects of Re number

The flows for all models corresponding to Re=100, 200 and 300 are simulated assuming 50% degree of stenosis. No indication of asymmetry of flow exists as regards to the axis of the tube so the results are presented corresponding to a random plane containing the axis. The streamline patterns for the Casson model are shown in Figure 4 where the fashion of growth of the recirculation region with increasing Re is evident. The difference between the vortex-lengths for Re=100 and Re=200 seems to be the same as that between Re=200 and Re=300 and that applies to all model cases.

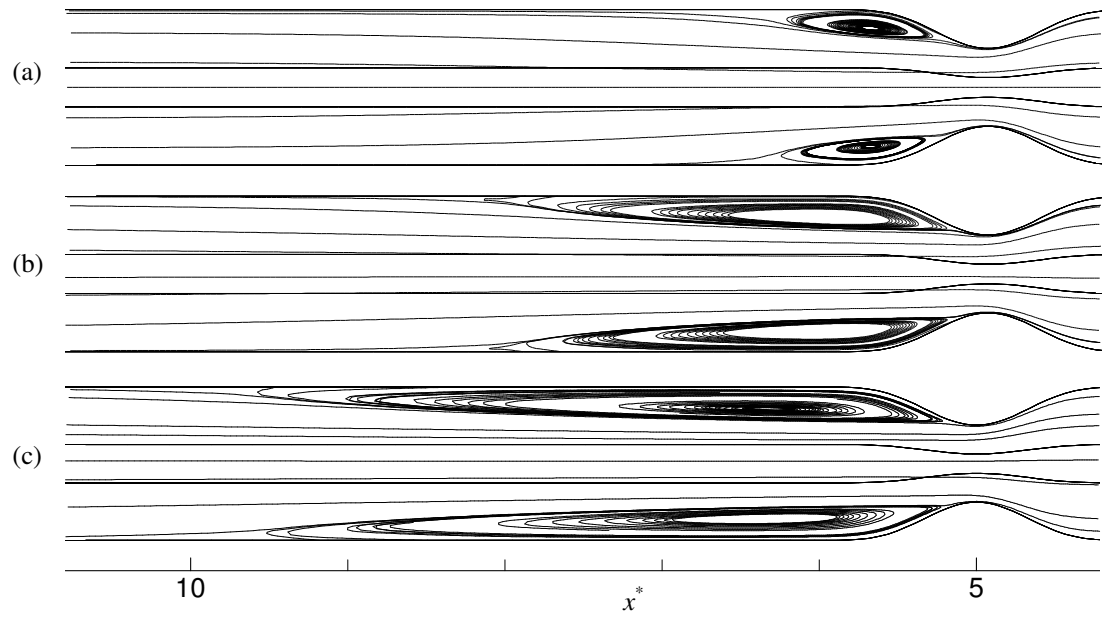

Figure 4: Streamlines for Casson- based flow for (a) Re=100; (b) Re=200; (c) Re=300 and for 50% degree of stenosis.

From the pressure-difference (ΔP) between inlet and outlet (Table 1) one can see that all Newtonian models cause higher pressure-difference than the Newtonian case and that implies

that a specific pressure difference would induce lower flow rates for the non-Newtonian models. In particular the highest ΔP is induced by the Power-Law model followed by the Casson and then the Quemada models. The change from Re=100 to Re=200 seems to induce the same rise to ΔP as the change from Re=200 to Re=300 for all models. Furthermore, the difference between ΔP values for every model at a specific Re seems to be the same for all three Re values.

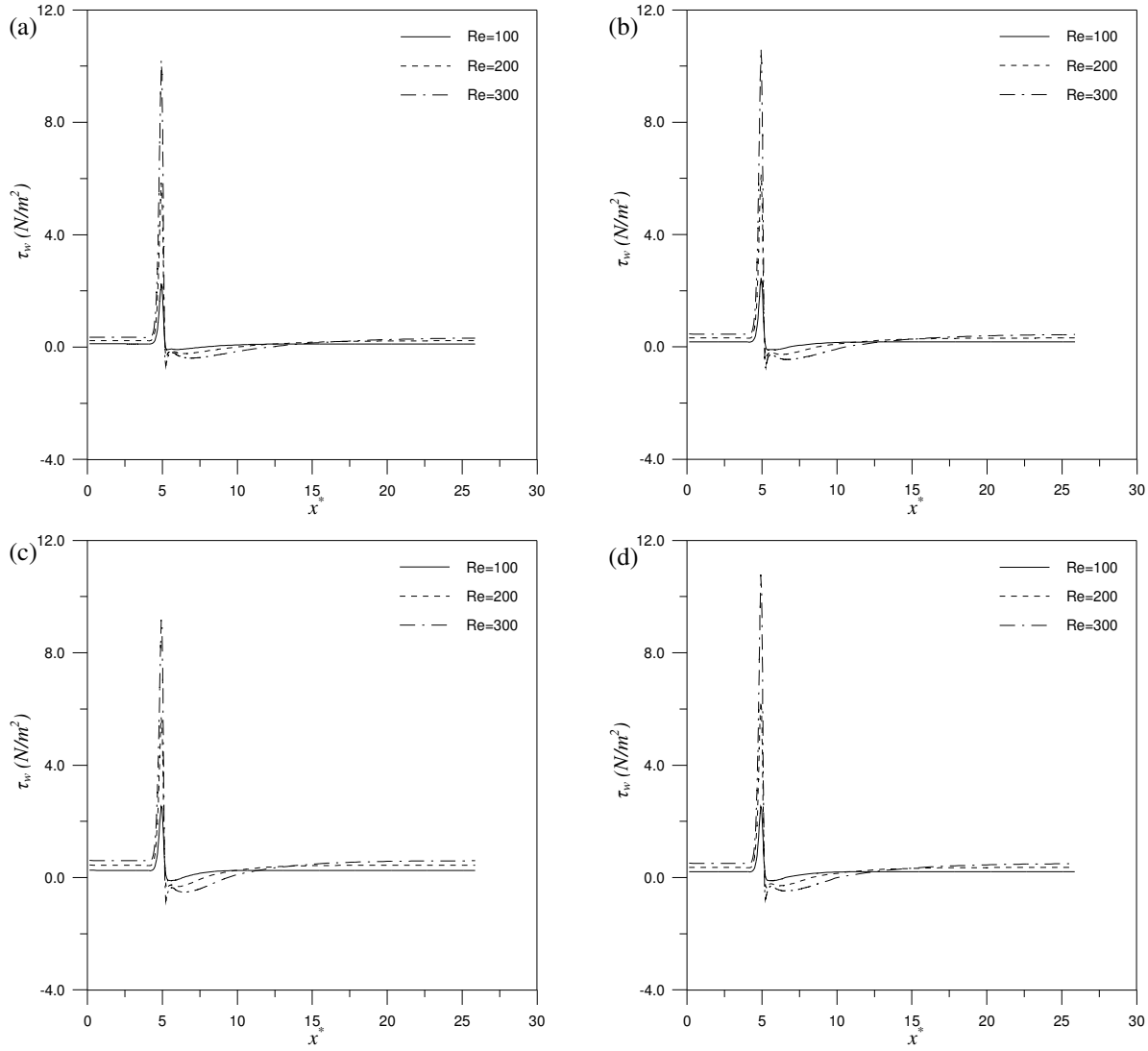

Figure 5: WSS distribution for different Re numbers for (a) Newtonian; (b) Casson; (c) Power-Law and (d) Quemada models.

The distribution of the WSS is one of the most important flow aspects due to its direct relevance to atherosclerosis formation [18]. The distribution of the x-wise component of the

WSS is shown in Figure 5 for all models. A prominent positive peak of the distribution is evident at the throat of the constriction, the value of which increases with increasing Re. The peak is followed by negative values indicating the presence of the recirculation region and gradually the WSS restores its undisturbed value. The maximum (τ_w^{max}) and minimum (τ_w^{min}) values of the distribution are shown in Table 2 for all models. For Re=100 the values of τ_w^{min} and τ_w^{max} are very close for all models and higher in absolute compared to the Newtonian case. As Re increases the effect differences between the models become more marked and in particular τ_w^{max} for the Power-Law model is lower compared to the rest of the models. This is induced from the lower viscosity that the Power-Law model exhibits for the high shear-rates occurring at the throat of the constriction due to the velocity gradients becoming more intense for higher Re. The value of τ_w^{max} for the Power-Law model also differs markedly from the other models for higher Re.

		Newtonian	Casson	Power-Law	Quemada
St=20%	Re=100	12.57	22.62	27.54	19.26
St=50%	Re=100	21.17	31.55	36.52	28.06
St=50%	Re=200	53.05	66.41	72.99	62.02
St=50%	Re=300	95.67	110.39	115.30	105.54
St=80%	Re=100	487.25	493.99	424.83	491.49

Table 1: Pressure difference (in N/m^2) for the various cases.

4.2 Effects of degree of stenosis

The flows for all models corresponding to Re=100 and degrees of stenosis equal to 20%, 50% and 80% are simulated. The streamlines for the Casson model in Figure 6 show the marked effects that the degree of stenosis has on the flow field. Whereas for 20% stenosis there is no vortex formed and even for 50% stenosis there is a small recirculation zone, for 80% stenosis the recirculation zone is dominant in the flow field.

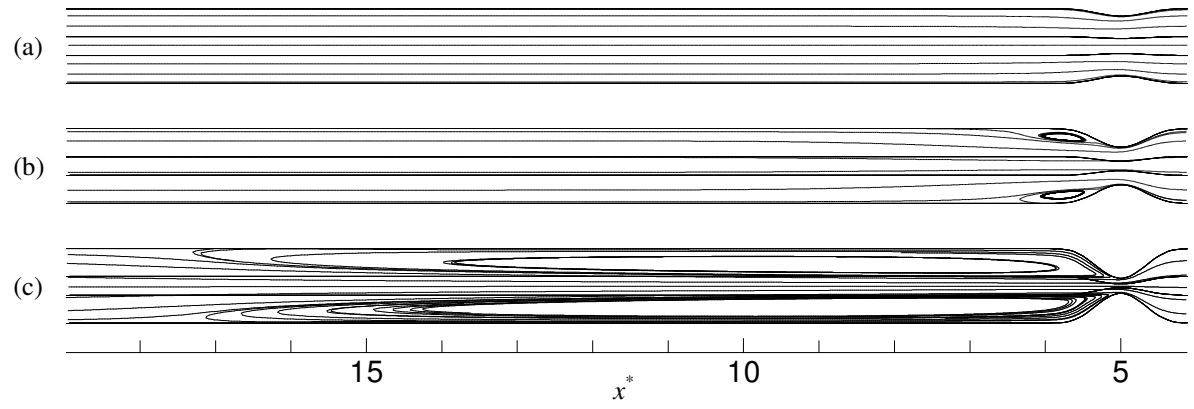

Figure 6: Streamlines for Casson- based flow at Re=100 and for different degrees of stenosis: (a) 20%; (b) 50%; (c) 80%.

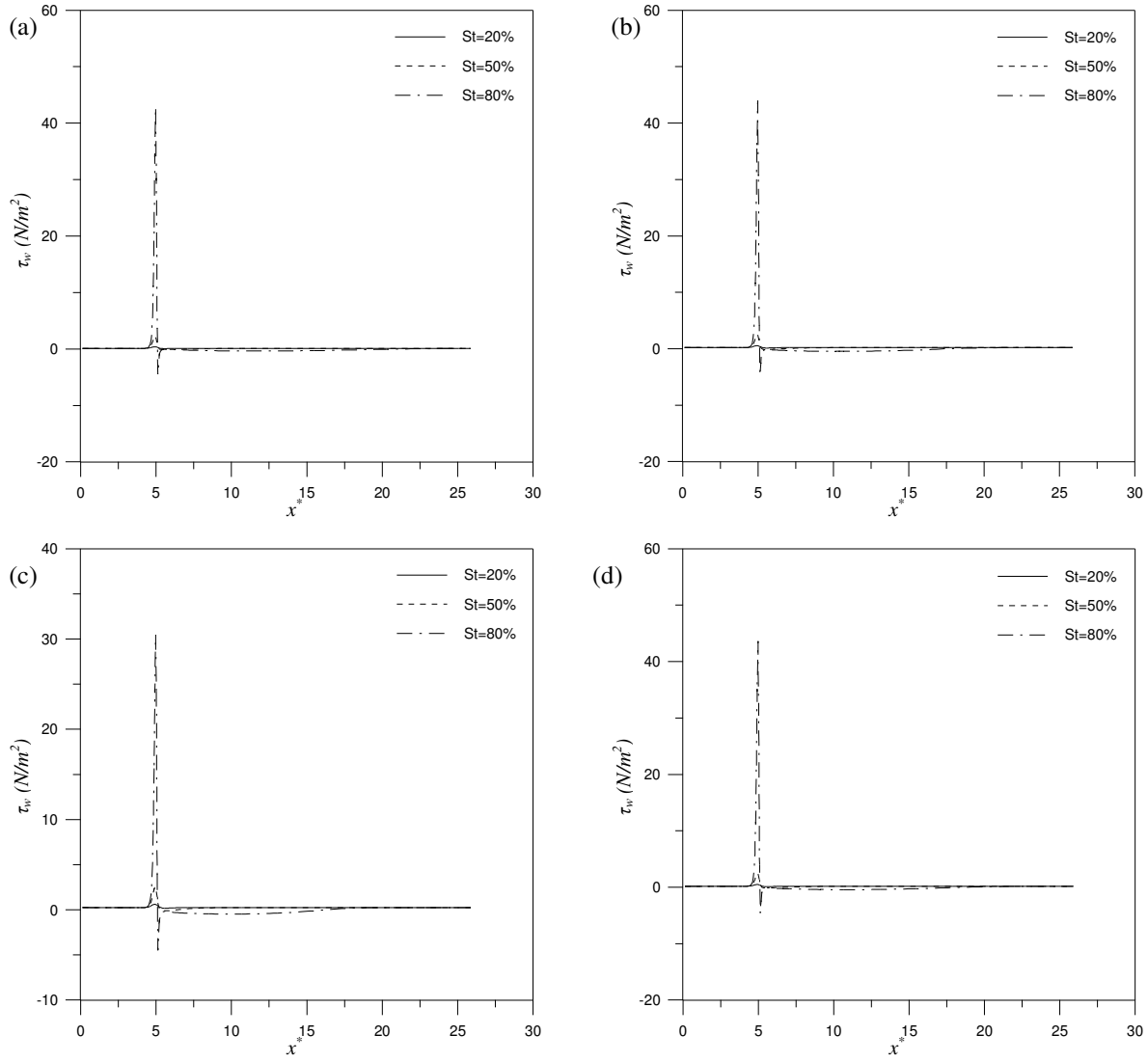

Figure 7: WSS distribution for different degrees of stenosis for (a) Newtonian; (b) Casson; (c) Power-Law and (d) Quemada models

The different impact that the severity of the stenosis has on the different model flows is more evident in the ΔP results (Table 1). It can be seen that although for St=20% the value of ΔP is the highest for the Power-Law model followed by the Casson and then the Quemada models, it becomes the lowest for St=80%. Taking into account that the pressure-difference is the integral of the WSS over the entire wall of the tube, this phenomenon is directly attributed to the low peak of WSS at the throat of the stenosis that the Power-Law model exhibits compared to the other models (Fig. 7). The Quemada and Casson models show similar trends for all degrees of stenosis. This can also be seen in Table 2 in addition with the results for τ_w^{min}. The latter is at the same levels for all models when a recirculation zone is formed

(St=50%, St=80%). It is worthwhile mentioning that for a change of 30% in the degree of stenosis from 50% to 80% the increase in τ_w^{max} is approximately 10 times greater than for the same change from 20% to 50% for all models.

		Newtonian		Casson		Power-Law		Quemada	
St	Re	τ_W^{min}	τ_W^{max}	τ_W^{min}	τ_W^{max}	τ_W^{min}	τ_W^{max}	τ_W^{min}	τ_W^{max}
20%	100	4.89e-2	0.380	0.125	0.523	0.162	0.593	9.88e-2	0.477
50%	100	-8.63e-2	2.26	-0.110	2.53	-0.108	2.54	-0.102	2.45
50%	200	-0.309	5.84	-0.351	6.27	-0.369	5.70	-0.334	6.14
50%	300	-0.668	10.21	-0.776	10.78	-0.846	9.17	-0.742	10.61
80%	100	-4.42	42.83	-4.58	43.94	-4.48	30.45	-4.54	43.59

Table 2: Minimum and maximum wall shear-stress (in N/m^2) for the various cases.

5 CONCLUSIONS

A study of the flow effects of three different blood rheological models namely the Casson, Power-Law and Quemada models in a three-dimensional model of an axisymmetric stenosis is presented. The flow field and wall shear-stress distributions that each model induces for different Re number and degrees of stenosis is investigated and results show that there are marked differences between simulating the blood as Newtonian and as non-Newtonian fluid. Furthermore, the Power-Law model exhibit similar trends as the Quemada and Casson models as regards to the pressure difference when Re alters whereas this trend is different as regards to the WSS. For low degrees of stenosis the pressure difference and WSS peaks for the Power-Law model are higher than for the other models. This phenomenon reverses for high degrees of stenosis. Quemada and Casson models exhibit similar behaviour for the variety of Re numbers and degrees of stenosis studied.

ACKNOWLEDGEMENT

The financial support by the Greek General Secretariat for Research and Technology under the contract 01EP24 is gratefully acknowledged.

REFERENCES

[1] K. C. Ang and J. N. Mazumdar. Mathematical modelling of three-dimensional flow through an asymmetric arterial stenosis. *Mathl. Comput. Modelling*, **25**, 19-29, 1997.

[2] A. S. Dvinsky and M. Ojha. Simulation of three-dimensional pulsatile flow through an asymmetric stenosis. *Medical & Biological Engineering & Computing*, **32**, 138-142, 1994.

[3] B. Bethier, R. Bouzerar and C. Legallais. Blood flow patterns in an anatomically realistic coronary vessel: influence of three reconstruction methods. *J. Biomechanics*, **35**, 1347-1356, 2002.

[4] Q. Long, X. Y. Xu, K. V. Ranmarine, P. Hoskins. Numerical investigation of physiologically realistic pulsatile flow through arterial stenoses. *J. Biomechanics*, **34**, 1229-1242, 2001.

[5] D. Tang, C. Yang, S. Kobayashi and D. N. Ku. Generized finite difference method for 3-D viscous flow in stenotic tubes with large wall deformation and collapse. *Applied Numerical Mathematics*, **38**, 49-68, 2001.

[6] V. Deplano and M. Siouffi. Experimental and numerical study of pulsatile flows through stenosis: Wall shear stress analysis. *J. Biomechanics*, **32**, 1081-1090, 1999.

[7] D. Bluestein, C. Gutierrez, M. Londono and R. T. Schoephoerster. Vortex shedding in steady flow through a model of an arterial stenosis and its relevance to mural platelet deposition. *Annals of Biomedical Engng.*, **27**, 763-773, 1999.

[8] J. R. Buchanan Jr., C. Kleinstreuer and J. K. Comer. Rheological effects on pulsatile hemodynamics in a stenosed tube. *Computers & Fluids*, **29**, 695-724, 2000.

[9] G. Pontrelli. Blood flow through an axisymmetric stenosis. *Proc. Instn Mech Engrs Part H - J. of Engineering in Medicine*, **215,** 1-10, 2001

[10] P. Neofytou and D. Drikakis. Effects of blood models on flows through a stenosis. *International Journal for Numerical Methods in Fluids*, **43**, 597-635, 2003.

[11] N. A. Casson. *A flow equation for pigment-oil suspensions of the printing ink type*. In: Rheology of Disperse Systems, pp. 84-102. C.C. Mills (Ed.). Pergamon Press, New York, 1959.

[12] F. J. Walburn and D. J. Schneck. A constitutive equation for whole human blood. *Biorheology*, **13**, 201-210, 1976.

[13] D. Quemada. Rheology of Concentrated Disperse systems III. General features of the proposed non-newtonian model. Comparison with experimental data. *Rheologica Acta*, **17**, 643-653, 1977.

[14] T. C. Papanastasiou. Flow of materials with yield. *Journal of Rheology*, **31**, 385-404, 1987.

[15] S. E. Charm, W. McComis and G. Kurland. Rheology and structure of blood suspension. *J. Appl. Physiol*, **19**, 127-133, 1964.

[16] P. Neofytou and D. Drikakis. Non-Newtonian flow instability in a channel with a sudden expansion. *Journal of Non-Newtonian Fluid Mechanics*, **111**, 127-150, 2003.

[17] B. P. Leonard. A stable and accurate convective modelling procedure based on quadradic upstream interpolation. *Comp Meth Appl Mech Engng*, **19**, 59-98, 1979.

[18] P. F. Davies. Flow-meditated endothelial mechanotransduction. *Physiological Reviews* **75**, 519-560, 1995.